

## Chapter 1

### Early thermalization, hydrodynamics and energy loss in AdS/CFT

Paul M. Chesler

*Department of Physics, Harvard University, Cambridge, MA 02138, USA*

Wilke van der Schee

*MIT Center for Theoretical Physics, Cambridge, MA 02139, USA*

Gauge/gravity duality has provided unprecedented opportunities to study dynamics in certain strongly coupled gauge theories. This review aims to highlight several applications to heavy ion collisions including far-from-equilibrium dynamics, hydrodynamics and jet energy loss at strong coupling.

#### 1. Introduction

Gauge/gravity duality equates certain gauge theories with theories of quantum gravity in one higher dimension.<sup>1</sup> This extra dimension has a natural interpretation as the renormalization group scale, and has led to the name “holographic duality.” In the limit where the gauge theory is strongly coupled and has a large number of colors  $N_c$  the dual description reduces to classical supergravity. Hence, challenging strongly coupled quantum dynamics in the gauge theory can be accessed by solving classical partial differential equations. All physics — from microscopic interactions to macroscopic hydrodynamics — is encoded in the dual classical dynamics. Holography can thereby provide systematic and controlled access to strongly coupled dynamics via the solution to the classical partial differential equations. Currently there is no other theoretical tool capable of accessing strongly coupled real-time dynamics in a controlled setting.

Heavy ion collisions at RHIC and the LHC have demonstrated that the produced quark-gluon plasma is strongly coupled.<sup>2</sup> Hence it is of interest to model heavy ion collisions using holography. However, while there exists many theories with dual gravitational descriptions — some with QCD-like features such as confinement and chiral symmetry breaking<sup>3,4</sup> — the dual description of QCD is not known (if it exists). Nevertheless, given the immense challenge of studying strongly coupled dynamics in QCD it is invaluable to have a model where strongly coupled dynamics can be studied in a controlled systematic setting. This is especially true if the results are valid for a class of strongly coupled gauge theories and hence have some degree of universality.

In this review we shall focus on the simplest theory with a holographic dual: 3+1 dimensional super-Yang-Mills theory with four supersymmetries ( $\mathcal{N} = 4$  SYM). In the limit where the SYM is strongly coupled and has a large number of colors  $N_c$  the dual description reduces to classical supergravity in asymptotically five dimensional Anti-de Sitter spacetime  $AdS_5$ <sup>1</sup> (see also<sup>5,6</sup>). While the ground state of SYM is very different from QCD — SYM is conformal and contains no particles whereas QCD is confining and has a rich spectrum of hadrons — at temperatures not too far above the deconfinement transition both theories consist of strongly coupled non-Abelian plasmas. It is in this setting where dynamics in SYM can potentially provide lessons for dynamics in QCD.

In what follows we highlight insights obtained via holography in three settings. First, we discuss relativistic hydrodynamics including computations of the shear viscosity at strong coupling and the construction of causal viscous hydrodynamics. We then discuss far-from-equilibrium dynamics and the collisions of shock waves in SYM and their application to early time dynamics in heavy-ion collisions. Finally, we give a brief review of progress made in jet quenching and energy loss at strong coupling.

## 2. First successes: viscosity and relativistic hydrodynamics

### 2.1. Viscosity from black hole horizons

Gauge/gravity duality provides a very natural way to describe thermal states: they are described by black holes, which are the simplest stationary states in  $AdS_5$  gravity with a notion of temperature. This temperature is simply the black hole's Hawking temperature.<sup>7</sup> The topology of the horizon is inherited from the gauge theory, where a thermal state usually is extended infinitely; this is one major difference from ordinary black holes in our universe, and in fact these black holes in  $AdS_5$  are more appropriately called black branes. Another major difference is the boundary of the  $AdS_5$  spacetime, which can be thought of as the place where the gauge theory lives. This boundary reflects back the thermal radiation, and the black branes are hence in stable thermal equilibrium, as opposed to black holes in flat spacetime, which evaporate away<sup>a</sup>.

It is also possible to construct gradient expansion solutions to Einstein's equations, where the local geometry is approximately that of boosted black brane with slowly varying temperature and boost velocity.<sup>8,9</sup> In this case the corresponding dual gauge theory state is that of a system in local thermal equilibrium with dynamics governed by hydrodynamics. Simply put, in the limit of slowly varying fields Einstein's equations reduce to hydrodynamics in one less dimension. The

<sup>a</sup>Also, black holes in our universe tend to have very small temperatures of order of mK, as black holes of higher temperature are hard to form and would quickly evaporate. The thermal stability of black holes in  $AdS$  allows any temperature, and in fact the temperature of black holes representing a quark-gluon plasma would have the same very high temperature of order  $10^{12}$ K.

connection between slowly varying solutions to Einstein's equations and hydrodynamics is known as the fluid/gravity correspondence. By matching the gradient expansion obtained by solving Einstein's equations to the constitutive relations of hydrodynamics, transport coefficients such as the viscosity can be computed at strong coupling.

At first order in gradients the constitutive relation for the stress tensor  $T^{\mu\nu}$  in relativistic neutral hydrodynamics read<sup>10</sup>

$$T_{\mu\nu} = e u_\mu u_\nu + p[e] \Delta_{\mu\nu} + \pi_{\mu\nu}, \text{ where,} \quad (1)$$

$$\Delta_{\mu\nu} = g_{\mu\nu} + u_\mu u_\nu \text{ and} \quad (2)$$

$$\pi_{\mu\nu} = -\eta[e] \sigma_{\mu\nu} - \zeta[e] \Delta_{\mu\nu} (\nabla \cdot u) + \mathcal{O}(\partial^2), \text{ with} \quad (3)$$

$$\sigma_{\mu\nu} = \Delta_{\mu\alpha} \Delta_{\nu\beta} (\nabla^\mu u^\nu + \nabla^\nu u^\mu) - \frac{2}{3} \Delta_{\mu\nu} \Delta_{\alpha\beta} \nabla^\alpha u^\beta, \quad (4)$$

where  $e$  is the proper energy density,  $u_\mu$  the fluid velocity,  $p[e]$  is the pressure (which is a function of the proper energy via an equation of state),  $\pi_{\mu\nu}$  is the shear tensor,  $\eta$  the shear viscosity and  $\zeta$  is the bulk viscosity, which vanishes in scale invariant theories such as SYM. Note that the fluid velocity and energy density are defined as the time-like eigenvector and associated eigenvalue of the stress tensor ( $T_{\mu\nu} u^\nu = -e u_\mu$ ) and that  $\sigma^{\mu\nu}$  is transverse and traceless:  $u^\mu \sigma_{\mu\nu} = \sigma_\mu^\mu = 0$ . Alternatively one can say that the fluid velocity is defined such that when boosting  $T_{\mu\nu}$  with velocity  $u_\mu$  there is no momentum flow, i.e.  $T'_{0i} = 0$ , which is called the Landau frame<sup>b</sup>. The conservation equation  $\nabla^\mu T_{\mu\nu} = 0$  together with the equation of state and the viscosity (computed theoretically or measured) now form a closed system of equations, fully determined by a given initial energy density and fluid velocity.

The equation of state, viscosity and higher order transport coefficients are not determined by hydrodynamics itself, and are a property of the microscopic theory under consideration. In weakly coupled QCD it is possible to use the Boltzmann equation to perturbatively compute the shear viscosity, which led to<sup>12</sup>

$$\eta_{\text{weak}} = \kappa \frac{T^3}{g^4 \log(1/g)} + \mathcal{O}\left(\frac{1}{g^4}\right), \quad (5)$$

with  $T$  the temperature,  $g$  the gauge coupling and  $\kappa$  a coefficient depending on the number of colors and flavors, which can be computed numerically. Non-perturbatively it is unknown how to compute the viscosity of QCD. However, there have been attempts to compute the viscosity using lattice techniques (see<sup>13</sup> for a review). It was therefore ground-breaking when a few years after the discovery of gauge/gravity duality Policastro, Son and Starinets computed the shear viscosity of a thermal plasma described by strongly coupled SYM theory:<sup>14</sup>

$$\eta = \frac{s}{4\pi} = \frac{\pi}{8} N_c^2 T^3, \quad (6)$$

<sup>b</sup>When including a charge density with corresponding current and chemical potential it is also possible to define a frame where there is no charge flow, which is called the Eckart frame.<sup>11</sup> In this review we do not include a charge density.

with  $s$  is the entropy density. The factor of  $1/4\pi$  is surprisingly universal and valid for any strong coupling and large  $N_c$  quantum field theory with a gravitational dual. For instance adding charge density changes both the shear viscosity and the entropy density, but its ratio is still  $1/4\pi$ .

Nevertheless, it is possible to have holographic models with different viscosity to entropy ratios, most notably by including higher derivative corrections in the Einstein equations. In this case corrections for finite  $N_c$  can actually make the  $\eta/s$  ratio drop below  $1/4\pi$ , thereby violating the conjectured universal lower bound<sup>15</sup> on the viscosity.<sup>16</sup> Nevertheless, general considerations using the quantum mechanical uncertainty principle still hint at the existence of a lower bound, even though its value is likely smaller than  $1/4\pi$ .

Holography can also yield finite coupling and finite  $N_c$  corrections to the viscosity. For SYM the results read:<sup>17–19</sup>

$$\eta/s = \frac{1}{4\pi} \left( 1 + \frac{15}{\lambda^{3/2}} \zeta(3) + \frac{5}{16} \frac{\lambda^{1/2}}{N_c^2} \right), \quad (7)$$

with  $\lambda = g^2 N_c$  the 't Hooft coupling. As expected from (5) the viscosity increases as the coupling constant decreases, and the increase can be significant at reasonable values of the coupling constant (for  $\lambda \sim 20$  and  $N_c \sim 3$  the corrections both are roughly 20%). Current hydrodynamic models of the quark-gluon plasma indeed favor an  $\eta/s$  in the range  $1/4\pi$  to  $2.5/4\pi$ .<sup>20–23</sup>

## 2.2. Second order relativistic hydrodynamics

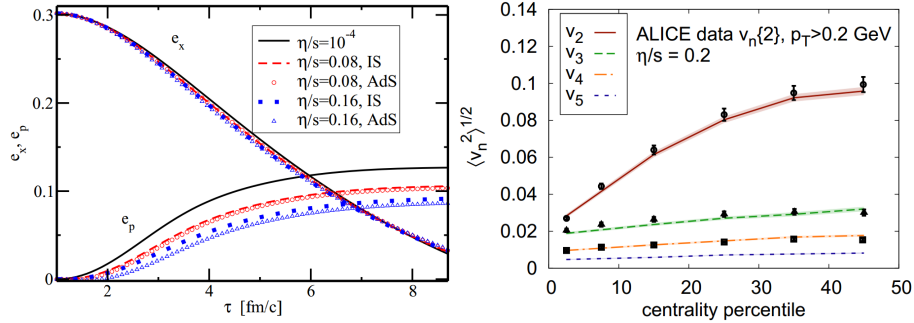


Figure 1. (left) The second order hydrodynamics derived using AdS/CFT (AdS) is compared with the older weakly coupled Muller-Israel-Stewart hydrodynamics (IS), which uses  $\tau_\pi = 6\eta/sT$  and does not include the  $\lambda_1$  or  $\lambda_2$  in eqn. 8. For these initial conditions the spatial and momentum anisotropy ( $e_x$  and  $e_p$ ) do not depend much on the precise value of the second order transport coefficients (figure from<sup>24</sup>). (right) Similar hydrodynamics has been used to obtain recent viscosity over entropy ratios of roughly 0.12 and 0.2 at top RHIC and LHC collisions respectively (LHC estimate shown, figure from<sup>23</sup>).

Holography and in particular the fluid/gravity duality also has led to a more systematic understanding of (relativistic) hydrodynamics itself.<sup>8,25,26</sup> As alluded to above,

via the fluid/gravity correspondence it is possible to systematically solve Einstein's equations. The gradient expansion solution encodes the constitutive relations of hydrodynamics to *all orders* in gradients and associated transport coefficients.<sup>8,25</sup> Let us begin by simply stating the results of<sup>8,25</sup> for the shear tensor  $\pi^{\mu\nu}$  up to the second order in gradients.

Since SYM is conformal, to write  $\pi^{\mu\nu}$  at second order in gradients it is useful to employ derivative operators  $\mathcal{D}_\mu$  which transform covariantly under conformal transformations. For tensors  $Q_{\nu\cdots}^{\mu\cdots}$  which, under a conformal transformation  $g_{\mu\nu} \rightarrow e^{2\phi}\tilde{g}_{\mu\nu}$ , transform like  $Q_{\nu\cdots}^{\mu\cdots} = e^{-w\phi}\tilde{Q}_{\nu\cdots}^{\mu\cdots}$ ,  $\mathcal{D}$  is defined by<sup>26</sup>

$$\begin{aligned}\mathcal{D}_\sigma Q_{\nu\cdots}^{\mu\cdots} &\equiv \partial_\sigma Q_{\nu\cdots}^{\mu\cdots} + w \mathcal{A}_\sigma Q_{\nu\cdots}^{\mu\cdots} + \gamma_{\sigma\lambda}^\mu Q_{\nu\cdots}^{\lambda\cdots} + \cdots - \gamma_{\sigma\nu}^\lambda Q_{\lambda\cdots}^{\mu\cdots} - \cdots, \\ \gamma_{\mu\nu}^\lambda &\equiv g_{\mu\nu} A^\lambda - \delta_\mu^\lambda A_\nu - \delta_\nu^\lambda A_\mu, \\ A_\mu &\equiv u^\nu \partial_\nu u_\mu - \frac{\partial_\nu u^\nu}{3} u_\mu.\end{aligned}$$

With this definition derivatives transform covariantly:  $\mathcal{D}_\lambda Q_{\nu\cdots}^{\mu\cdots} = e^{-w\phi}\mathcal{D}_\lambda \tilde{Q}_{\nu\cdots}^{\mu\cdots}$ , and for instance Eq. (4) simplifies to  $\sigma_{\mu\nu} = \mathcal{D}_\mu u_\nu + \mathcal{D}_\nu u_\mu$ . The full second order conformal shear tensor is now given by<sup>c</sup>:

$$\begin{aligned}\pi_{\mu\nu} &= -\eta \sigma_{\mu\nu} + \eta \tau_\pi u^\lambda \mathcal{D}_\lambda \sigma_{\mu\nu} + \lambda_1 [\sigma_{\mu\lambda} \sigma_\nu^\lambda - \frac{\Delta_{\mu\nu}}{3} \sigma^{\alpha\beta} \sigma_{\alpha\beta}] \\ &\quad + \lambda_2 [\omega_{\mu\lambda} \sigma_\nu^\lambda + \omega_{\nu\lambda} \sigma_\mu^\lambda] + \lambda_3 [\omega_{\mu\lambda} \omega_\nu^\lambda + \frac{\Delta_{\mu\nu}}{3} \omega^{\alpha\beta} \omega_{\alpha\beta}],\end{aligned}\quad (8)$$

where  $\omega_{\mu\nu} = \mathcal{D}_\mu u_\nu - \mathcal{D}_\nu u_\mu$ . In strongly coupled SYM the second order transport coefficients are given by  $\tau_\pi = (2 - \ln(2))/2\pi T$ ,  $\lambda_1 = \eta/2\pi T = 2\lambda_2/\ln(2)$  and  $\lambda_3 = 0$ .<sup>8</sup> Note that all these coefficients get considerably more complicated when including a chemical potential; in particular  $\lambda_3$  becomes non-zero.<sup>27</sup>

Second order hydrodynamics is particularly useful for numerical simulations of viscous hydrodynamics. This is because high momentum modes in first order relativistic hydrodynamics can propagate faster than the speed of light. Fundamentally this is not a problem, as hydrodynamics is an expansion in long wavelengths, i.e. small momenta, and these acausal modes are outside the regime of its applicability.<sup>28</sup> Nevertheless, these modes make the equations numerically unstable<sup>29</sup> and therefore in numerical simulations a second order term was added to stabilize the equations, giving Muller-Israel-Stewart hydrodynamics.<sup>30,31</sup>

Muller-Israel-Stewart hydrodynamics can be seen as a special case of second order hydrodynamics where  $\lambda_i = 0$ . One insight which holography helped solidify is that, in contrast to the Muller-Israel-Stewart theory, at a given order in the gradient expansion one must add every possible tensor structure to the constitutive relations which is consistent with the symmetries of the underlying quantum field theory. This had lead to the development of causal viscous relativistic hydrodynamics.<sup>24,32,33</sup> In

<sup>c</sup>Most of these computations have been done for fluids living in a curved spacetime,<sup>25</sup> which gives an extra term not considered in this review.

conformal theories such as SYM the equations of second order hydrodynamics give causal propagation for high momenta modes.

While the second order transport coefficients make simulations much easier to perform, the precise value of these coefficients fortunately does not seem to have a big influence on the particle spectra in realistic simulations (see figure 1, left). The latter feature does however crucially depend on using conformal hydrodynamic equations; when using (second order) non-conformal equations results do seem to depend on the second order coefficients.<sup>34</sup> One of the biggest successes of these equations are estimates for the shear viscosity of the quark-gluon plasma,<sup>20–23</sup> as shown in Fig. 1 (right).

Another more recent example of a better understanding of hydrodynamics comes from,<sup>35</sup> where in a specific boost-invariant setting all transport coefficients were computed numerically up to order 240 in the gradient expansion. With those coefficients it could be shown that the hydrodynamic gradient expansion is not necessarily convergent, it was found to be an asymptotic series. Moreover, it was understood why hydrodynamics did not converge, since the divergent hydrodynamic expansion contains information about the non-hydrodynamic modes. Within AdS/CFT these modes are included in the so-called quasi-normal modes: vibrations of the black hole horizon. Strikingly, by a Borel resummation reference<sup>35</sup> was able to extract the precise value of the dominant quasi-normal mode from the hydrodynamic expansion, thereby showing how hydrodynamics contains information about its own break-down.

Much work has been devoted to study charged hydrodynamics, extending the previous formulas to a plasma with a conserved current, chemical potential and various new transport coefficients, see for instance.<sup>27,36</sup> More recently there has been interest in anomalous hydrodynamics, where quantum anomalies lead to modified hydrodynamic equations. A plasma with a non-trivial axial charge density will develop an electric current  $\vec{J}$  in the direction of an external magnetic field  $\vec{B}$  (chiral magnetic effect or CME):<sup>37,38</sup>

$$\vec{J} = \frac{e^2}{2\pi^2} \mu_5 \vec{B}, \quad (9)$$

where  $\mu_5$  is the chemical potential associated with the axial charge. For averaged heavy ion events  $\mu_5$  would be zero, but a full event-by-event anomalous hydrodynamic simulation suggests that this effect is measurable in heavy ion collisions.<sup>39</sup> Similarly to the analysis above, also for the CME holography has proved extremely useful to show how this effect is in fact necessarily included already in first order charged hydrodynamics, and also to estimate the relevant transport coefficients at strong coupling.<sup>40,41</sup>

Lastly, inspiration from the symmetries present in AdS has led to non-trivial analytic solutions of the hydrodynamic equations. An interesting solution was provided by Gubser,<sup>42</sup> where a solution to viscous conformal hydrodynamics with boost-invariance and a non-trivial expansion in the transverse plane was found.

This solution follows from a simple set-up in AdS, but then leads to this non-trivial analytic and hence very useful hydrodynamic solution. Recently, this approach has been extended to an exact solution of the relativistic Boltzmann equation.<sup>43</sup>

Interestingly, aside from the computation of transport coefficients, much of the development in hydrodynamics above need not rely on gauge/gravity duality. Nevertheless, inspiration from the duality has led to this more precise understanding of hydrodynamics, by using gauge/gravity as a theoretical arena to get new insights.

### 3. Fast thermalization and the resulting stress tensor

#### 3.1. Simple models

Perhaps an even more remarkable feature of holography is the straightforward possibility to study far-from-equilibrium dynamics in strongly coupled gauge theories. How do non-equilibrium systems thermalize and relax to local equilibrium? Using holography answering this question amounts to studying real time dynamics in the gravitational dual, which is not much different from conventional problems in general relativity, such as binary neutron stars, or black hole inspirals.<sup>44,45</sup> As is well-known these latter problems can still be very challenging from a numerical point of view, but compared to non-perturbative quantum field theory it is definitely an enormous simplification. For a review of the use of numerical relativity in holography see for example.<sup>46</sup>

The first studies of holographic thermalization computed how perturbed black holes relax to homogeneous black holes, computing the so-called quasi-normal modes.<sup>47</sup> These are determined by expanding the perturbation of the metric in a sum of modes proportional to  $e^{-i\omega_i t}$ , with complex frequency  $\omega_i$ . The Einstein equations and boundary conditions at the horizon and boundary then dictate that there is a discrete spectrum, whereby the mode always decays (i.e.  $\Im(\omega_i) < 0$ ). The mode with the slowest decay will then determine the late-time decay back to the thermal black hole, and hence can be said to determine the thermalization time in this setting. Dimensional analysis in this scale invariant theory dictates that  $\omega_i \sim T$ , but the coefficient has to be computed numerically, giving  $\Im(\omega_0) \approx 8.6T$ .<sup>47</sup>

The estimate from quasi-normal modes could imply a thermalization time  $t_{\text{therm}} < 1/T$ , which for a temperature of 1000 MeV would be about 0.2 fm/c. Compared to perturbative methods this is very fast, which should be expected for a system at strong coupling. On the other hand, even though the coupling is assumed to be infinite, there is still a finite answer for the thermalization time, leading to the intuition that strong interactions still have some microscopic physics present as the scale  $1/T$ .

Nevertheless, the the quasi-normal mode analysis is only valid near equilibrium: the state is assumed to be a small perturbation of the final thermal state. In heavy ion collisions the initial state is very far-from-equilibrium, so solving the full non-linear Einstein equations is of great importance. One of the first studies solving this

numerically is presented in,<sup>48,49</sup> where quark-gluon plasma formation and thermalization was studied in both homogeneous and boost invariant set-ups (see fig. 2). The gauge theory dynamics was, by symmetry, effectively 1+0 dimensional and the dual gravitational dynamics was 1+1 dimensional. In these papers non-equilibrium states were created by starting in the ground state and turning on background fields. It was found that even in the case where the initial state is the vacuum, a thermal state can be achieved in times of order  $1/T$  with  $T$  the final state temperature.

An intriguing finding in<sup>49</sup> was that when the system first starts to behave hydrodynamically, viscous effects were order one: the first order viscous correction to the constitutive relations (1) is as big as the leading term. Nevertheless, even with such large viscous corrections the hydrodynamic gradient expansion was seen to be well behaved. Moreover, the applicability of hydrodynamics was seen not to be governed by convergence of the hydrodynamic gradient expansion. Instead, the applicability of hydrodynamics was seen to be governed by the decay of non-hydrodynamic degrees of freedom.

The approach in<sup>49</sup> was extended in.<sup>50</sup> Here the main feature was the possibility to chose several initial states and to evolve them without turning on any background fields. For all initial states they found a thermalization time less than  $1/T$ , with  $T$  the temperature at the moment of thermalization.

Of particular utility, this paper also introduced a dimensionless quantity,  $F(w) \equiv \frac{\tau}{w} \partial_\tau w$ , where  $w \equiv T_{eff} \tau$  can be thought of as dimensionless time and  $T_{eff}$  is the temperature associated with the energy density at that time. The dimensionless function  $F(w)$  is completely determined within hydrodynamics and for instance equals  $2/3$  for ideal hydrodynamics. As  $F(w)$  is unique within hydrodynamics it is clear that differences between  $F(w)$  found for the different evolutions in AdS/CFT must be due to genuine non-hydrodynamic effects, as is convincingly shown on the left of Fig. 3.

The right of figure 3 shows a similar study in a homogeneous setting, with more than 1000 initial states, also leading to thermalization within a time of  $1/T$ .<sup>51,52</sup> The main new result in this paper was to compare the full non-linear thermalization process with the linearized quasi-normal mode approach outlined in the second paragraph of this section. Quite surprisingly it was found that for general initial states the evolution was always well described, within 20%, by the linearized approximation. This then also confirmed that the quasi-normal mode estimates of strongly coupled thermalization times were indeed accurate also at the non-linear level.

Lastly, these studies can be corrected for finite coupling effects, which has recently been done in.<sup>53,54</sup> Not surprisingly, finite coupling corrections slow down the thermalization, as in these papers becomes apparent through a smaller imaginary part of the lowest quasi-normal mode.



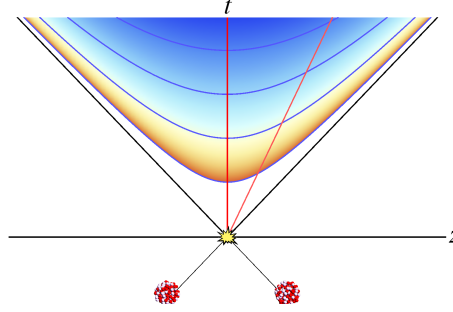


Figure 2. A simple and often used model of a heavy-ion collision was proposed by Bjorken,<sup>55</sup> where he assumed that a heavy-ion collision is approximately boost-invariant, at least near  $z = 0$ . This means that all physics only depends on proper time  $\tau = \sqrt{t^2 - z^2}$ , and hence that all physics experienced by observers, such as a temperature field illustrated here, is independent of its frame. The two red lines would illustrate two such frames, which indeed has equal temperatures at equal  $\tau$  (figure from<sup>56</sup>).

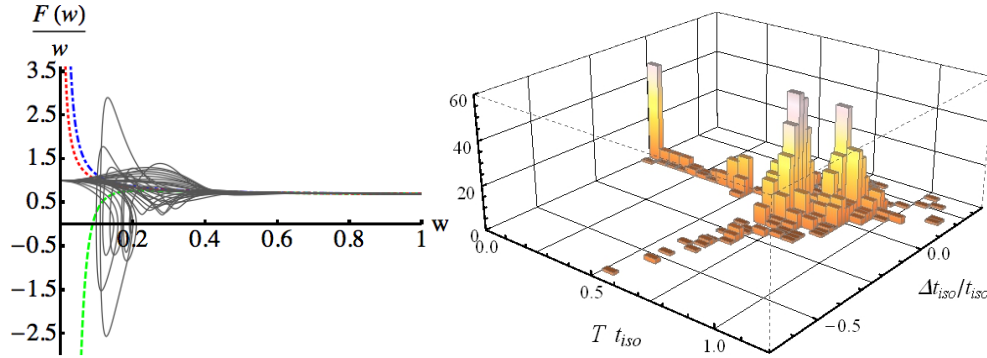


Figure 3. The left figure shows boost invariant thermalization, where the evolution of 29 random initial states of  $F(w) \equiv \frac{\tau}{w} \partial_\tau w$  as a function of  $w \equiv T_{eff} \tau$  is compared with predictions from first-, second- and third-order hydrodynamics (figure from<sup>50</sup>). It can be seen that they all thermalize in a time where  $\tau \lesssim 0.5/T_{eff}$ , where  $T_{eff}$  is the temperature associated with the energy density at that time. The right figure did a similar analysis in a homogeneous set-up, using over 1000 initial states. Also there thermalization always happens within  $t \lesssim 1/T$ . Here it is also shown that the difference between the linearized and fully non-linear Einstein equations is small, almost always less than 20% (figure from<sup>51</sup>).

### 3.2. Colliding shock waves

All models presented above contained enough spacetime symmetry to make the gauge theory dynamics effectively 1 + 0 dimensional. Here we shall review results where the gauge theory dynamics are allowed to be 1 + 1 and 1 + 2 dimensional. In holography the energy-momentum in the gauge theory directly corresponds to the metric in the gravitational theory, so to simulate highly energetic colliding nuclei it is therefore natural to consider collisions of gravitational shock waves, moving at the speed of light.<sup>57–62</sup> The shock waves can be viewed as analogous to the shock

waves constructed in flat space by Dray and 't Hooft,<sup>63</sup> which consist of taking a Schwarzschild black hole and boosting this to the speed of light, keeping its total energy fixed. The shock waves are dual to lumps of energy in the gauge theory, which propagate at the speed of light. When the shock waves collide they can produce a black hole which will then relax to equilibrium. Likewise, in the dual gauge theory, the collision will result in the formation of a non-Abelian plasma which will subsequently thermalize.

One interesting result from the aforementioned studies of shock wave collisions was the entropy production, estimated by the area of the trapped surface of the formed black hole at the time of collision. This trapped surface gives a lower bound on the area of the black hole horizon, which is directly related to the produced entropy in the gauge theory. Ref.<sup>59</sup> estimated that:

$$S \geq S_{trapped} \approx 35000 \left( \frac{\sqrt{s_{NN}}}{200 \text{ GeV}} \right)^{2/3}, \quad (10)$$

where  $S$  is the entropy produced in a central gold nucleus-nucleus collision with a nucleon-nucleon collision of energy  $\sqrt{s_{NN}}$  and  $S_{trapped}$  is the entropy of the trapped surface. The entropy increase during the evolution of the quark-gluon plasma is not too big due too to the relatively small viscosity, but can in fact be sizable as highly anisotropic plasmas increase the entropy production. Nevertheless Eq. (10) gives a lower bound on the final entropy produced, which is directly related to the measurable total charged particle multiplicity  $N_{tot,ch} = S/7.5$ .<sup>64</sup> In<sup>56</sup> the estimate (10) was made somewhat stronger by doing calculations numerically till later times, but two important features remained. Firstly the numerical value is about right for RHIC collisions, albeit on the high side, which is impressive as Eq. (10) is a direct calculation, without having any input from other experiments. Secondly, the  $2/3$  power law as a function of  $\sqrt{s_{NN}}$  is a robust outcome of a scale invariant theory. Nevertheless, with the LHC results now known,<sup>65</sup> the experimental data favors a power of  $1/2$ , and Eq. (10) therefore overestimated the multiplicity at LHC collisions. This can be taken as an indication that QCD is not scale invariant at energies probed between RHIC and LHC.

The previous calculations could not say much about the dynamics after the collision, which requires solving the full non-linear Einstein equations. It was therefore a major breakthrough when a real collision could be simulated within gravity.<sup>66</sup> This study collides planar gravitational shock waves, thereby simplifying the problem by neglecting transverse dynamics. The initial conditions for the shock wave are determined by the stress tensor

$$T_{\pm\pm}(z_{\pm}) = \kappa h(z_{\pm}), \quad (11)$$

where  $z_{\pm} = t \pm z$  are null coordinates along the collision axis and  $\kappa = N_c^2/2\pi^2$  is a measure of the degrees of freedom of the gauge theory. All other components of the stress tensor are zero, and within pure gravity this fully determines the metric

before the collision. For this review we restrict  $h$  to be Gaussian:

$$h(z) = \frac{\mu^3}{w\sqrt{2\pi}} \exp\left[-\frac{z^2}{2w^2}\right], \quad (12)$$

where  $w$  is the width of the Gaussian and  $\kappa\mu^3 = \kappa \int_{-\infty}^{\infty} h(z)dz$  is the total energy per transverse area.

In what follows we make the following choices for parameters. We choose  $N_c = 1.8$  such that the ratio  $e/T^4 \approx 12$  matches lattice QCD simulations.<sup>59</sup> The choice of  $N_c < 3$  compensates for the fact that SYM has approximately three times as many degrees of freedom than QCD. We then fix  $\mu$  by setting the

$$\kappa\mu^3 \approx \frac{\sqrt{s_{NN}}}{2} \frac{N_{\text{Pb}}}{\pi R^2}, \quad (13)$$

where  $N_{\text{Pb}} = 206$  and  $R = 6$  fm. The right hand side of this equation is simply the energy density per unit area near the center of a lead nucleus. We choose the width of the Gaussian to be  $w \approx \frac{4}{3} R m_N / \sqrt{s_{NN}}$ , with  $m_N$  the nucleon mass. Of course real nuclei are not Gaussians, (nor is QCD = SYM) so all these numbers have to be taken with a grain of salt. Nevertheless, these choices gives a qualitative understanding of the scales in the problem.

After setting up these initial conditions it is possible to numerically solve the Einstein equations (see<sup>46,56</sup> for an introduction), and thereafter extract the expectation value of the gauge theory stress tensor. Figure 4 shows the energy density obtained in this way for collisions having  $\sqrt{s_{NN}} = 19.3$  GeV and  $\sqrt{s_{NN}} = 2.76$  TeV. For a proper comparison with<sup>66,67</sup> one should notice that the dimensionless product

$$\mu w = \left( \frac{\sqrt{s_{NN}}}{2\kappa} \frac{N_{\text{lead}}}{\pi R^2} \right)^{1/3} \frac{4}{3} R m_N / \sqrt{s_{NN}} \approx 23 (\sqrt{s_{NN}}/\text{GeV})^{-2/3}, \quad (14)$$

so that 19.3 GeV and 2.76 TeV correspond to a  $\mu w$  of 3.2 and 0.11 respectively, whereby we stress once more that these are ballpark figures, which we think are helpful for a useful comparison of gauge/gravity results to actual heavy ion collisions.

Several curious features are visible in the resulting energy density.<sup>67</sup> Firstly, for the low energy collisions the peak energy density is about 60% higher than the sum of the incoming energies. This is interpreted as a ‘pile-up’ of energy, as the shocks thermalize during the collision. For high energy shocks there is not enough time for this effect, and the shocks therefore only lose there energy gradually to the plasma, as well as forming a transient region of negative energy density, where it is not even possible to define a local rest frame.<sup>68</sup> Curiously, for the high energy shocks there seems to be a reasonably accurate analytic formulation — at least at small rapidities — by using a complexified boost symmetry, even valid in the far-from-equilibrium regime.<sup>69</sup> At later times the low and high energy collisions behave similarly though; they both thermalize fast (shown in figure 5) and deposit all their energy into the plasma.

Interestingly, the formed plasma is quite insensitive to the profile of the initial shocks, provided characteristic length of the profile is not too big.<sup>70</sup> This makes

the local energy density of the resulting plasma robust at least for thin and hence high energy shocks. The rapidity profile of these collisions may even be universal at strong coupling, and is therefore of considerable interest (figure 6, right). The left part of that figure displays the similar profile for low energy collisions, which looks similar in shape, but with a width that becomes smaller as the collision energy decreases.

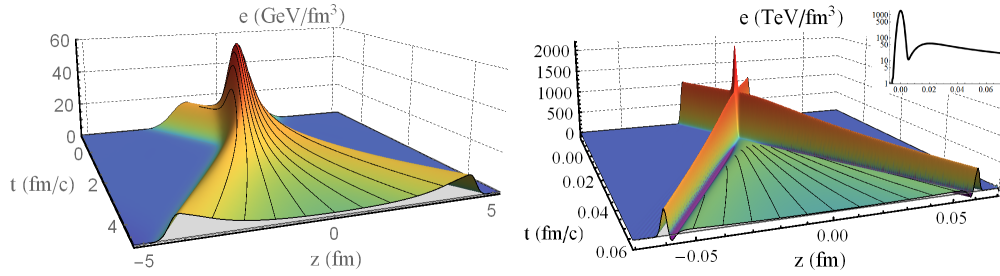


Figure 4. Energy density  $e$  for collisions of shock waves at low energy ( $\sqrt{s_{NN}} = 19.3$  GeV, left) and high energy ( $\sqrt{s_{NN}} = 2.76$  TeV, right) as a function of time and longitudinal coordinate  $z$ . The grey planes lie at the origin of the vertical axes. Note that these simulations are planar in the transverse plane and therefore neglect transverse dynamics. For the short time scales presented at the right plot this is probably a good approximation, but the simulation on the left will change when taking transverse expansion into account as well (figures adapted from<sup>67</sup>).

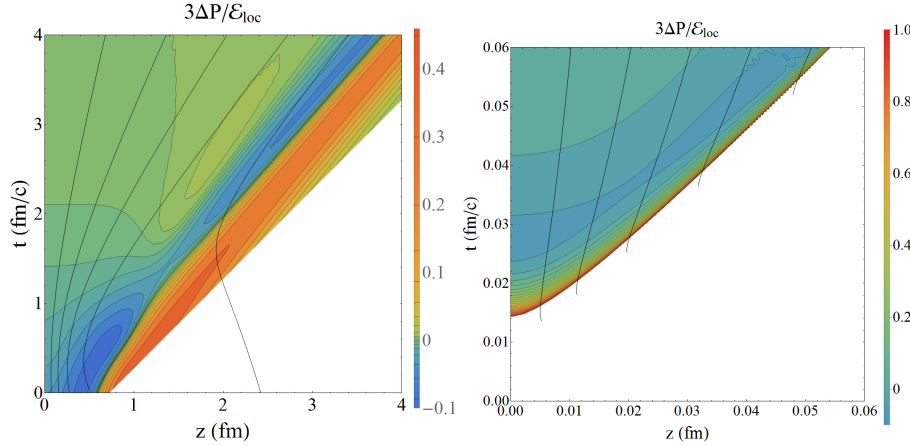


Figure 5.  $3\Delta\mathcal{P}_L^{\text{loc}}/\epsilon_{\text{loc}}$  for low (left) and high (right) energy shocks, with  $\Delta P$  the difference between the longitudinal pressure from holography, and the one computed using eqn. 1. The white areas indicate regions outside the light cone or where hydrodynamics deviates by more than 100%. The black lines are again stream lines, which for the high energy shocks stop at the region where no local rest frame exists.<sup>68</sup>

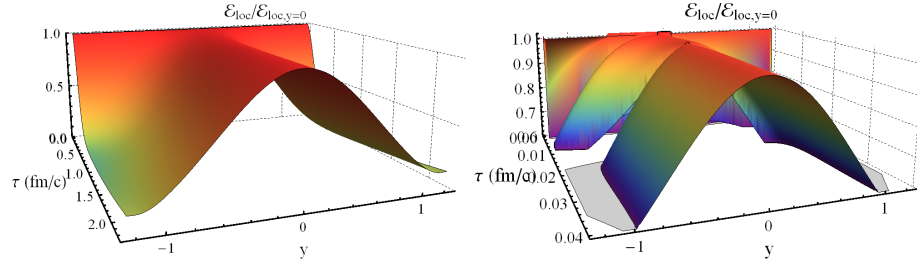


Figure 6. Energy density in the local rest frame around mid-rapidity as a function of spacetime rapidity  $y$  and proper time  $\tau$  for thick (left) and thin (right) shocks (the same shocks as figure 4). In the right case we have excluded from the plot the region in which the local rest frame is not defined because  $2|s| > |e + P_L|$  (figures adapted from<sup>67</sup>).

### 3.3. Including transverse dynamics

Lastly, we would like to mention that it is also possible to include transverse dynamics. Transverse expansion is essential during the late time of the QGPs explosion, but also early time initial velocities in the transverse plane influence the transverse momenta spectra. Nevertheless, a full shock wave collision with transverse expansion requires a 3+1 dimensional code in AdS spacetime, as there is always the extra AdS direction. As this can be technically complicated it is therefore natural to first try to include transverse dependence while assuming boost invariance in the longitudinal direction.

Assuming boost invariance is a bit subtle, as Fig. 6 convincingly shows a significant dependence on rapidity. Also, using proper time as a variable usually necessitates to start the gravitational simulation a finite time after the collision (see<sup>71</sup> for a counter example though), which has to be accompanied by an assumption on the dynamics before this time (early time expansion in the case to be presented). Nevertheless, starting the simulation at such a finite time with several simple profiles gave two lessons.<sup>72,73</sup> Firstly the plasma again thermalized fast, at a similar time scale as the examples above. Secondly, after the thermalization the transverse velocity was given to a good approximation by the following approximation:<sup>73,74</sup>

$$v_i = -0.33\tau \partial_i e / e, \quad (15)$$

with  $\tau$  the proper time, and  $e$  the local energy density in the transverse plane. This formula is in spirit similar to the universal pre-flow found in,<sup>75</sup> but note that only the flux is universal in the sense of that paper, whereas here we are interested in the local fluid velocity, which depends on the pressures as well.

Using these simulations it was then possible to couple this to relatively standard hydrodynamic and cascade codes, and thereafter obtain the full transverse momenta spectra at mid-rapidity for a central collision, which fits data surprisingly well (figure 7). Recently this has also been extended to several other systems, most notably also computing the measurable HBT radii.<sup>74</sup>

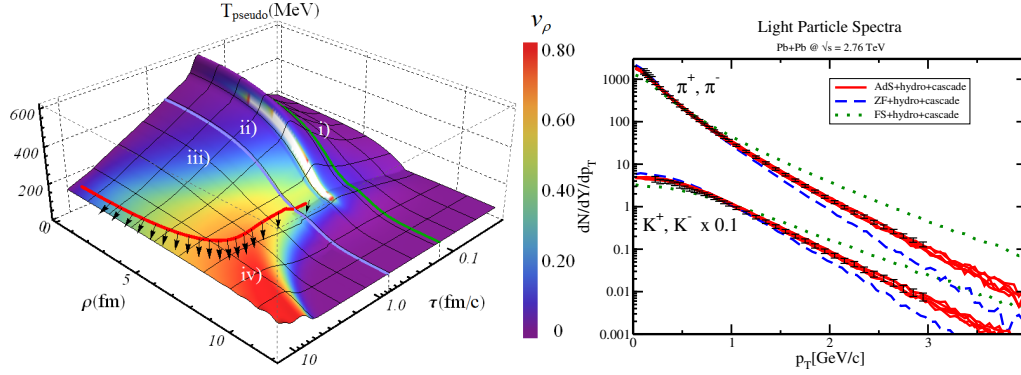


Figure 7. From the local energy density we plot the temperature (assuming equilibrium, therefore labeled  $T_{\text{pseudo}}$ ) and the radial velocity  $v_\rho = u_\rho/u_\tau$  for a representative simulation. The plot illustrates four physical tools used: i) early time expansion, ii) numerical AdS evolution, iii) viscous hydrodynamics until  $T = 0.17$  GeV, iv) kinetic theory after conversion into particles (indicated by arrows). The right plot shows the resulting particle spectra for pions and kaons, and also includes curves for a zero flow model (ZF) with  $v_i = 0$  until  $\tau = 1.0$  fm/c, and a free streaming model (FS), with zero longitudinal pressure (figure from,<sup>73</sup> experimental data from ALICE<sup>76</sup>).

## 4. Jet energy loss

### 4.1. Are there jets at strong coupling?

During the early stages of heavy-ion collisions — in which the energy density is the highest — energetic partons can be created via hard processes. The resulting excitations — jets — consist of collimated sprays of energy and can traverse the fireball while depositing energy and momentum into the medium. Analysis of the particle correlations in the produced jets can provide useful information about the dynamics of the plasma including the rates of energy loss and momentum broadening.<sup>77–80</sup>

Why study jets and energy loss at strong coupling? One piece of evidence that the quark-gluon plasma produced in heavy-ion collision is strongly coupled comes from jet quenching itself.<sup>81–83</sup> Jets traversing the fireball appear to lose their energy very quickly, indicating strong interactions with the medium.

A natural process by which jets can be created is the decay of off-shell particles such as photons. At weak coupling the decay leads to well-collimated sprays of energy with the polarization of the photon imprinting itself in the final state in a so called “antenna pattern” (see for example<sup>84</sup> and references therein). However, at strong coupling the situation is very different: the decay of off-shell photons leads to states which are spherically symmetric (in the rest frame of the off-shell photon): all correlation functions at spatial infinity are spherically symmetric and there are no well collimated sprays of energy.<sup>85</sup>

What does this mean for studying jets at strong coupling? Does the observed isotropy mean there are no jets at strong coupling? Where does the isotropy come from? In other words, at what stage in the evolution does the isotropy develop?

Does it come from the underlying photon decay or from the subsequent late time evolution as the energy propagates outward to infinity?

In order to understand the above issues it was useful to study the propagation of radiation in strongly coupled holographic gauge theories. A simple setting to study this problem is that of radiation produced by an accelerated quark in strongly coupled conformal field theories. If one takes a heavy quark and accelerates it along some given trajectory, what does the pattern of emitted radiation look like? This problem is analogous to textbook studies of radiation produced by an accelerated charge in classical electrodynamics. However, instead of radiation carried by a classical  $U(1)$  gauge field, the radiation is that of a strongly coupled non-Abelian quantum field theory. Is the emitted radiation isotropic at strong coupling? If not, does it isotropize as it propagates to infinity?

This problem was studied in.<sup>86,87</sup> There it was found that the radiation produced by the accelerated quark is not isotropic. Nor does the radiation isotropize as it propagates out to infinity. Remarkably, the angular distribution of power produced by an accelerated quark is the same at weak and strong coupling! This suggests that the isotropy observed in the decay of off-shell photons at strong coupling comes from the production mechanism itself — *i.e.* the decay — and not the subsequent evolution.

The lesson from this is that one should not treat the jet production mechanism with strong coupling tools. Indeed, in asymptotically free QCD it is natural to expect the production mechanism during the early stages of heavy ion collisions to be governed by weakly coupled physics. Ideally, one should treat the initial hard physics with perturbative QCD and then study soft processes such as energy loss with strongly coupled tools. Simply put, the utility of modeling jets with strongly coupled tools comes from studying their evolution and energy loss *after* they are produced.

#### **4.2. Holographic models of jets**

While at strong coupling it is impossible to create well collimated sprays of energy via off-shell photon decays, one can construct states at some initial time  $t = t_i$  which share features with jets created via weakly coupled processes. Namely, one can construct states with excitations which are well-collimated, have energy  $E \gg T$  with  $T$  the temperature of the plasma, and which can propagate very far through the plasma before thermalizing. Ideally, one would compute the initial state using perturbative QCD. However, we shall take a different approach and focus on universal features which are insensitive to the precise initial conditions used to construct the state at time  $t_i$ . These include the rates of energy loss and momentum broadening and the penetration depth defined as the total distance a jet can propagate through plasma before thermalizing.

Let us focus for simplicity on  $q\bar{q}$  jets in strongly coupled conformal field theories (for other holographic models of jets see for example<sup>88-91</sup>). According to

holographic duality a  $q\bar{q}$  pair moving through plasma is dual to a classical string moving through a black hole geometry.<sup>4</sup> The geometry dual to an infinite static plasma at temperature  $T$  is the AdS-Schwarzschild geometry, where the metric may be written

$$ds^2 = \frac{L^2}{u^2} \left[ -f(u)dt^2 + d\mathbf{x}^2 + \frac{du^2}{f(u)} \right], \quad (16)$$

where  $L$  is the AdS radius and  $f(u) = 1 - u^4/u_h^4$ . The horizon of the geometry is at radial coordinate  $u = u_h$  with  $u_h = 1/\pi T$ . The boundary of the geometry, which is where the dual field theory lives, is at radial coordinate  $u = 0$ .

As it evolves in time the string sweeps out a 1 + 1 dimensional *worldsheet*. Events on the worldsheet can be labeled by coordinates  $(\tau, \sigma)$  which are related to events in spacetime via the embedding functions  $X^M \equiv \{t(\tau, \sigma), \mathbf{x}(\tau, \sigma), u(\tau, \sigma)\}$ . The dynamics of the embedding functions are governed by the Nambu-Goto action

$$S = -T_0 \int d\tau d\sigma \sqrt{-\gamma}, \quad (17)$$

where the string tension is  $T_0 = \frac{\sqrt{\lambda}}{2\pi L^2}$  with  $\lambda$  the 't Hooft coupling and  $\gamma = \det \gamma_{ab}$  with

$$\gamma_{ab} = \partial_a X \cdot \partial_b X, \quad (18)$$

the worldsheet metric. Here and below the indices  $(a, b)$  run over the worldsheet coordinates  $\tau$  and  $\sigma$ . The action (17) is simply the area of the worldsheet.

Varying the action we obtain the string equations of motion

$$\partial_\tau \Pi_\mu^\tau + \partial_\sigma \Pi_\mu^\sigma, \quad (19)$$

where the string worldsheet currents  $\Pi_M^a$  are

$$\Pi_M^a = \frac{\delta S}{\delta(\partial_a X^M)} = -T_0 \sqrt{-\gamma} \gamma^{ab} g_{MN} \partial_a X^N, \quad (20)$$

where  $g_{MN}$  is the AdS-Schwarzschild metric and as usual  $\gamma^{ab}$  is the inverse of  $\gamma_{ab}$ . Note that the energy of the string is

$$E = - \int d\sigma \Pi_0^\tau. \quad (21)$$

The string equations of motion (19) are simply the equations of energy conservation on the worldsheet with  $\Pi_0^\sigma$  the energy flux down the string.

The endpoints of the string are charged under a bulk  $U(1)$  gauge field  $\mathcal{A}_M$ . The boundary of the AdS geometry behaves as an ideal conductor.<sup>92</sup> Hence the gauge field induces a current  $J^\mu$  on the boundary, which up to an overall sign has the interpretation as the baryon current of a *dressed* quark.<sup>92,93</sup> This is shown schematically in Fig. 8. Therefore, one can regard the spatial location of the string endpoint as roughly coinciding with the spatial location of the quarks. The boundary conditions at the string endpoints are set by the mass of the quark.<sup>4</sup> For infinitely massive



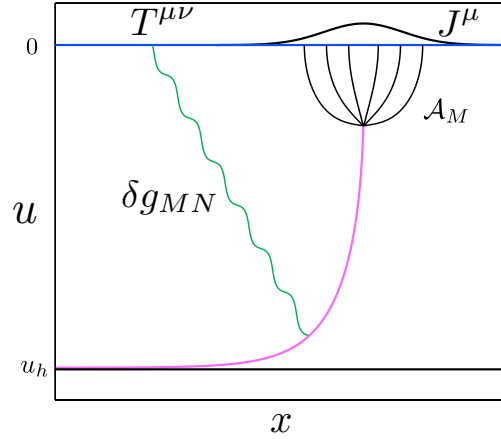


Figure 8. A cartoon showing a string at some fixed time in the AdS-Schwarzschild geometry. The endpoint of the string is charged under a  $U(1)$  gauge field  $\mathcal{A}_M$ . The boundary of the AdS-Schwarzschild geometry — located at radial coordinate  $u = 0$  — behaves as an electromagnetic conductor. Up to a minus sign the current  $J^\mu$  induced on the boundary has the physical interpretation as the baryon current of the quark. Likewise, via Einstein's equations the string perturbs the AdS-Schwarzschild geometry. The near-boundary behavior of the metric perturbation encodes the stress tensor  $T^{\mu\nu}$  of the jet.

quarks the endpoint is fixed at the boundary. Correspondingly, the current  $J^\mu$  is localized with delta function support. In contrast, for massless quarks the endpoints are free to fall in the AdS-Schwarzschild geometry. Likewise, the current  $J^\mu$  spreads out as the endpoints fall. For intermediate mass quarks the endpoint is fixed to be at some radial coordinate  $u_m$ .

Via Einstein's equations the presence of the string also perturbs the AdS-Schwarzschild geometry. Just as the near boundary behavior of the gauge field  $\mathcal{A}_M$  encodes the quark baryon current  $J^\mu$ , the near-boundary behavior of the metric perturbation  $\delta g_{MN}$  encodes the stress tensor  $T^{\mu\nu}$  of the system. This is also shown schematically in Fig. 8.

With the above preliminaries layed out, the basic strategy then will be to construct initial string data at some time  $t_i$  and evolve the string profile forward in time according to the string equations of motion (19). To echo the previous point, we seek strings whose boundary boundary energy density  $T^{00}$  is that of a well collimated spray of energy which propagates very far before thermalizing. We will then study jet quenching and other observables which are insensitive to the details of the precise form of the initial data. In what follows we will highlight results for infinitely massive quark jets and massless quark jets.

### 4.3. Heavy quark energy loss

One of the first studies<sup>94–96</sup> of energy loss via AdS/CFT came from the study of heavy quarks propagating at constant velocity  $v$  through a static box of plasma at temperature  $T$ . As the quark moves through the plasma it transfers energy and momentum to the plasma via frictional drag. Hence an external force is required to maintain constant velocity. This can be supplied by an electromagnetic field coupled to the quark's baryon current  $J^\mu$ .

Under the assumption that the quark has been dragged at constant velocity for an arbitrary duration of time, it is natural to seek a steady-state solution to the string equations of motion. Choosing worldsheet coordinates  $\tau = t$  and  $\sigma = u$  the steady-state ansatz take the form

$$x(t, u) = vt + vx_0(u), \quad (22)$$

with the endpoint terminating at the boundary  $u = 0$ . Solving the string equations of motion (19) for  $x_0(u)$  yields

$$x_0(u) = \frac{1}{2u_h} \left[ \tan^{-1} \frac{u}{u_h} + \frac{1}{2} \log \frac{u_h - u}{u_h + u} \right]. \quad (23)$$

We plot  $x_0(u)$  in Fig. 9.

The electromagnetic field dragging the quark (and hence the string endpoint) must be supplying energy at a rate equal to the rate energy is dissipated by drag. In the dual gravitational description the energy lost via drag is encoded by a flux of energy down the string towards the event horizon,  $\frac{dE}{dt} = \Pi_0^\sigma$ . Plugging the the solution (23) into Eq. (20), the drag reads<sup>94–96</sup>

$$\frac{dE}{dt} = \frac{\pi}{2} \sqrt{\lambda} T^2 \frac{v^2}{\sqrt{1-v^2}}. \quad (24)$$

Hence, as the 't Hooft coupling  $\lambda \rightarrow \infty$  the quark loses energy faster and faster.

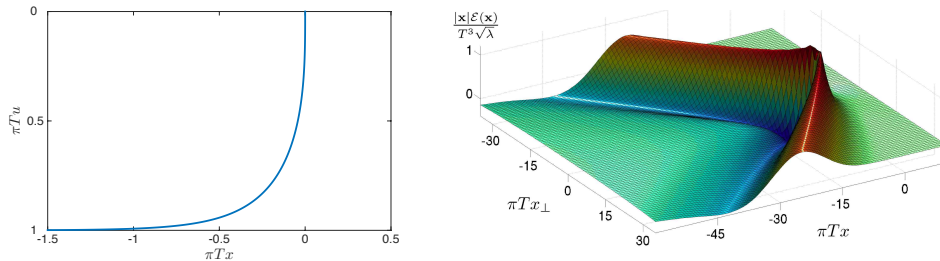


Figure 9. Left: the string profile (23) for a heavy quark. Right: the energy density produced by a heavy quark moving at three quarters the speed of light in the  $x$ -direction. A Mach cone is clearly present.

A natural question to ask is where does the energy lost by the quark go? To answer this question it is useful to study the stress tensor  $T^{\mu\nu}$ . This requires solving

Einstein's equations for the metric perturbation  $\delta g_{MN}$  due to the presence of the string and extracting the stress tensor from its near-boundary asymptotics. This calculation was carried out in.<sup>97–100</sup> In the right panel of Fig. 9 we also plot the normalized energy density  $\mathcal{E} \equiv \frac{2\pi^2}{N^2} T^{00}$  for a heavy quark moving in the  $x$ -direction at three quarters the speed of light. The speed of sound in a relativistic conformal field theory is  $c_s = 1/\sqrt{3} \approx 0.57$ . Hence the quark is moving supersonically. As is clear from the figure, the quark creates a Mach cone. Evidently, the energy lost via drag is carried away by sound waves.

There have since been numerous studies of heavy quark energy loss at strong coupling in more general settings. Some examples include heavy quark energy loss in non-conformal theories,<sup>101</sup> anisotropic plasmas<sup>102</sup> and in far-from-equilibrium states such as the shock wave collisions discussed above.<sup>103</sup> In the latter study it was demonstrated that even in far-from-equilibrium states, such as those produced by colliding shock waves, the equilibrium energy loss formula (24) provides a reasonable estimate of the heavy quark energy loss rate. Additionally, heavy quark energy loss due to deceleration (*i.e.* non steady-state) was studied in,<sup>104</sup> and the rates of heavy quark momentum broadening were studied in.<sup>105,106</sup>

## 5. Light quark energy loss

In contrast to strings dual to heavy quarks, where the endpoints are fixed to the AdS boundary, the endpoints of strings dual to massless quarks are allowed to fall unimpeded towards the event horizon of the AdS-Schwarzschild geometry.<sup>4,92</sup> For massless quarks the string equations of motion (19) must be solved subject to the open string boundary conditions

$$\Pi_M^r = 0 \text{ at the endpoints.} \quad (25)$$

The fact that string endpoints fall toward the horizon implies there does not exist steady-state solutions to the string equations of motion. Hence studying light quark energy loss is considerably more complicated than studying heavy quark energy loss. Nevertheless it is a straightforward matter to numerically solve the string equations of motion (19) with the open string boundary conditions (25). For details on how to do this see for example.<sup>93</sup>

In Fig. 10 we plot a numerically generated string profile at several values of fixed coordinate time  $t$ . At time  $t = 0$  the initial string profile is simply a point located at the AdS boundary  $u = 0$ . As time progresses the string expands from a point to an extended object and the endpoints fall towards the horizon. The endpoints travel a total distance  $x_{\text{stop}} \approx 10/\pi T$  before falling into the horizon. As the endpoint fall into the horizon, the boundary baryon current  $J^\mu$  (depicted schematically in Fig. 8) becomes delocalized and starts to evolve hydrodynamical according to the diffusion equation.<sup>92</sup> This corresponds to the thermalization of the light quark jet.

The total distance the string endpoints and hence the jet can travel depends on initial conditions. A natural question is for a fixed energy  $E$ , what is the maximum

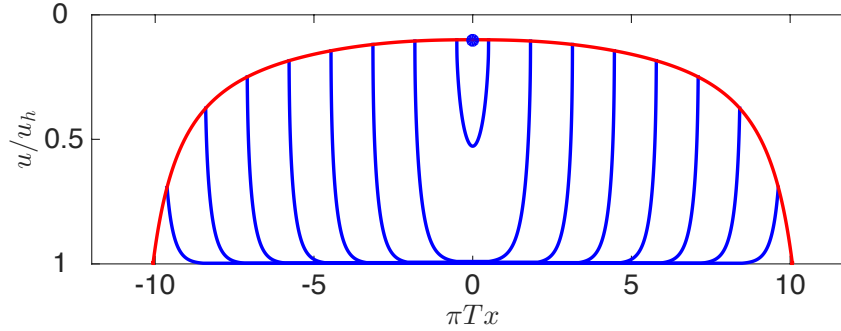


Figure 10. A numerically generated falling string profile dual to a light quark jet. The string is shown at several values of fixed coordinate time  $t$ . The string is created at the point  $x = u = 0$  and subsequently expands into an extended object. The red lines denote the string endpoint trajectories. The endpoints travel a distance  $x_{\text{stop}} \approx 10/\pi T$  before falling into the horizon at  $u = u_h$ .

distance the string endpoints can travel before falling into the horizon? In the language of the dual field theory, for fixed jet energy  $E$ , what is the maximum distance a light quark jet can travel before thermalizing? To answer this question one can numerically generate an ensemble of solutions to the string equations of motion (19) with different initial conditions. One can then compute the energy (21) and compare the stopping distance  $x_{\text{stop}}$  to  $E$ . This computation was carried out in<sup>93</sup> where it was found that the maximum distance a jet with energy  $E$  can travel before thermalizing is given by

$$x_{\text{stop}} = \frac{C}{T} \left( \frac{E}{T\sqrt{\lambda}} \right)^{1/3}, \quad (26)$$

where  $C \approx 0.526$ . The  $x_{\text{stop}} \sim E^{1/3}$  scaling was also found in.<sup>107</sup> The constant  $C$  was recently computed analytically and found to be<sup>108</sup>

$$C = \frac{2^{1/3} \Gamma(\frac{5}{4})}{\sqrt{\pi} \Gamma(\frac{3}{4})}. \quad (27)$$

We now turn to the light quark energy loss rate. Following,<sup>109</sup> we focus on strings whose  $x_{\text{stop}}$  is asymptotically large compared to  $1/T$ . Such strings have worldsheets which are approximately null.<sup>93,109</sup> Why? When  $x_{\text{stop}} \rightarrow \infty$  the scaling (26) requires  $E \rightarrow \infty$ . Since strings have finite tension the  $E \rightarrow \infty$  limit is generically realized by strings that expand at nearly the speed of light, meaning that the string profile must be approximately that of an expanding filament of null dust. Indeed, null strings have profiles  $X_{\text{null}}^M$  satisfying  $\gamma(X_{\text{null}}) = 0$  and from (20) have divergent energy density.

Since null strings satisfy  $\gamma(X_{\text{null}}) = 0$  they minimize the Nambu-Goto action (17) and are exact albeit singular solutions to the string equations of motion (19). Following,<sup>109</sup> to obtain finite energy solutions to the equations of motion one can

expand the string embedding functions about a null string solution

$$X^M = X_{\text{null}}^M + \epsilon \delta X_{(1)}^M + \epsilon^2 \delta X_{(2)}^M + \dots, \quad (28)$$

where  $\epsilon$  is a bookkeeping parameter (which can be set equal to 1 at the end of calculations). In what follows it is useful to choose worldsheet coordinates  $\tau = t$  and  $\sigma$  such that  $\dot{X}_{\text{null}} \cdot X'_{\text{null}} = 0$  and  $\delta X_{(m)} = \{0, \delta \mathbf{x}, 0\}$ . We denote the location of the string endpoints by  $\sigma = \sigma_*$ . The string equations of motion can then be solved perturbatively in powers of  $\epsilon$ .

Focusing on strings propagating in the  $x$ -direction, the null string embedding functions can be written

$$X_{\text{null}}^M = \{t, x_{\text{geo}}(t, \sigma), 0, 0, u_{\text{geo}}(t, \sigma)\}, \quad (29)$$

where for each  $\sigma$   $x_{\text{geo}}$  and  $u_{\text{geo}}$  satisfy the null geodesic equations, which read

$$\frac{\partial x_{\text{geo}}}{\partial t} = \frac{f}{\xi}, \quad (30)$$

$$\frac{\partial u_{\text{geo}}}{\partial t} = \frac{f \sqrt{\xi^2 - f}}{\xi}, \quad (31)$$

where  $\xi = \xi(\sigma)$ . The parameter  $\xi$  determines the initial inclination of the geodesics in the  $x - u$  plane and, more fundamentally, specifies the conserved spatial momentum associated with the geodesics,  $f(u)^{-1} \partial x_{\text{geo}} / \partial t = \xi^{-1}$ . The geodesic equations have the solution

$$x_{\text{geo}} = -\frac{u_h^2}{u_{\text{geo}}} {}_2F_1\left(\frac{1}{4}, \frac{1}{2}, \frac{5}{4}; \frac{u_h^4}{\zeta u_{\text{geo}}^4}\right) + C(\sigma) \quad (32)$$

where  ${}_2F_1$  is the Gauss hypergeometric function,  $\zeta \equiv 1/(1 - \xi^2)$  and  $C(\sigma)$  is an arbitrary function which can be chosen such that  $x_{\text{geo}}(t = 0, \sigma) = 0$ .

Henceforth let us focus on strings created at the point  $x = u = t = 0$  at the AdS boundary. At asymptotically early times  $t \ll u_h$ , when the string is close to the AdS boundary,  $f = 1$  and the geodesics are given by

$$x_{\text{geo}} = t \cos \sigma, \quad u_{\text{geo}} = t \sin \sigma. \quad (33)$$

Hence, the worldsheet coordinate  $\sigma$  is simply the initial angle of the geodesic in the  $x - u$  plane. Likewise,

$$\xi(\sigma) = \sec \sigma. \quad (34)$$

In Fig. 11 we plot a null string generated by a congruence of geodesics with  $\sigma_* = 0.025$ . The string profile, denoted by the blue curves, is shown at several values of coordinate time  $t$ . The string starts off at a point on the boundary and expands at the speed of light while falling towards the horizon. The rust colored curves represent the null geodesics that make up the string and the red curve is the endpoint trajectory. The total distance the string endpoint can travel is entirely controlled by the angle  $\sigma_*$ . As we elaborate on further below, in the limit  $\sigma_* \rightarrow 0$  the stopping distance diverges.

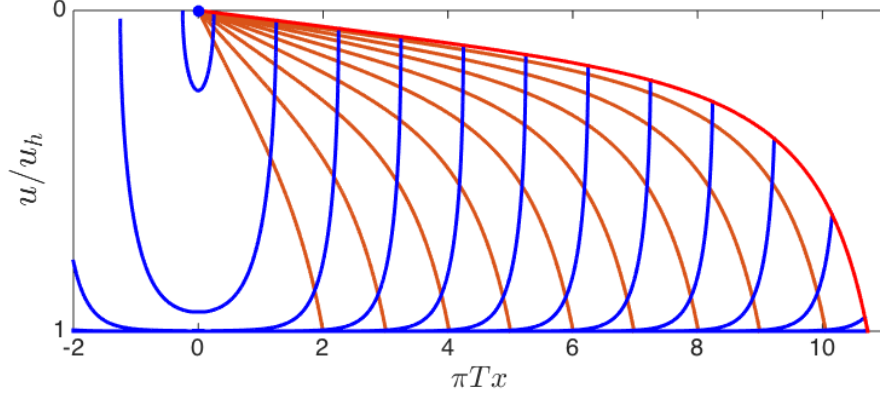


Figure 11. A null string (blue) shown at several different coordinate times  $t$ . The string starts off at a point on the boundary and expands at the speed of light while falling towards the horizon. The rust colored curves represent the null geodesics that make up the string and the red curve is the endpoint trajectory.

To study energy loss rate we must compute the first order corrections to the string embedding functions. At leading order in the bookkeeping parameter  $\epsilon$  the worldsheet energy density  $\Pi_0^\tau$  and flux  $\Pi_0^\sigma$  read

$$\Pi_0^\tau = -\frac{T_0 \xi \partial_\sigma u_{\text{geo}}}{u_{\text{geo}}^2} \sqrt{\frac{-\xi}{2\epsilon f \partial_t \delta x_{(1)}}} + O(\sqrt{\epsilon}), \quad \Pi_0^\sigma = O(\sqrt{\epsilon}). \quad (35)$$

Hence at leading order in  $\epsilon$  the string equations of motion (19) simply read  $\partial_t \Pi_0^0 = 0$  so  $\Pi_0^\tau = \Pi_0^\tau(\sigma)$ . In other words, energy is simply transported on the congruence of geodesics which make up the null string!

We define the energy

$$E(x) \equiv -\int_{\sigma_*}^{\sigma_H(x)} \Pi_0^0(\sigma), \quad (36)$$

where  $\sigma_H(x)$  is the  $\sigma$  corresponding to the geodesic which impacts the horizon at  $x$ . In particular,  $\sigma_H(x = x_{\text{stop}}) = \sigma_*$ . The energy  $E(x)$  is simply the total string energy that makes it past the point  $x$ . The energy loss rate per unit length is

$$\frac{dE}{dx} = -\Pi_0^\tau(\sigma_H(x)) \sigma'_H(x). \quad (37)$$

We discuss the precise boundary interpretation of  $dE/dx$  below. To compute  $dE/dx$  we must compute  $\Pi_0^\tau$  and  $\sigma_H(x)$ .

Because  $\Pi_0^\tau$  is time independent it is only necessary to compute it at an initial time. Near the AdS boundary, where  $f = 1$  and the geodesics are given by (33), the string equation of motion  $\partial_t \Pi_0^\tau = 0$  leads to the equation of motion for  $\delta x_{(1)}$

$$\partial_t^2 \delta x_{(1)} + \frac{2}{t} \partial_t \delta x_{(1)} = 0, \quad (38)$$

which has the solution

$$\delta x(t, \sigma) = \phi(\sigma) + \frac{1}{t}\psi(\sigma), \quad (39)$$

for arbitrary functions  $\phi(\sigma)$  and  $\psi(\sigma)$ . The open string boundary conditions (25) require  $\psi(\sigma_*) = 0$ .

Substituting the string solution (39) and the geodesic solution (33) and (34) into (35) we obtain

$$\Pi_0^\tau = -T_0 \csc^2 \sigma \sqrt{\frac{\csc 2\sigma \sin \sigma}{\epsilon \psi(\sigma)}} + O(\sqrt{\epsilon}). \quad (40)$$

With  $\Pi_0^\tau$  computed and the congruence of null geodesics specified we can now compute  $dE/dx$ . But what is  $\psi(\sigma)$ ! The energy loss rate depends on an arbitrary function. At first sight this seems like a disaster. Not only can we not describe the production mechanism of jets via holography but their energy loss rate, at least for massless jets, seems to be very sensitive to initial conditions. However, this grim diagnosis turns out to be incorrect: the ambiguities in the light quark energy loss rate are largely transient effects which die out over time scales of order  $1/T$ . These effects are negligible in the high energy limit when  $x_{\text{stop}} \rightarrow \infty$ .

Let us consider  $x_{\text{stop}} \rightarrow \infty$  limit with  $x/x_{\text{stop}}$  fixed and first compute  $\sigma_H(x)$ .  $\sigma_H(x)$  can be computed from the geodesics solution (32) by setting  $u_{\text{geo}} = u_h$  and solving the resulting transcendental equation for  $\sigma$ . With  $\xi$  given by (34) the resulting equation can be solved analytically in the limit  $\sigma \rightarrow 0$  (*i.e.* for geodesics which travel very far before falling into the horizon). The solution reads  $\sigma_H(x) = \frac{u_h^2 \Gamma(\frac{1}{4})^2}{16\pi x^2}$ . Likewise, setting  $\sigma_H(x = x_{\text{stop}}) = \sigma_*$ , we see that the stopping distance is related to  $\sigma_*$  via

$$x_{\text{stop}} = \frac{u_h \Gamma(\frac{1}{4})^2}{4\sqrt{\pi\sigma_*}}. \quad (41)$$

As previously advertised,  $x_{\text{stop}} \rightarrow \infty$  when  $\sigma_* \rightarrow 0$ . We therefore may write

$$\sigma_H(x) = \sigma_* \left( \frac{x_{\text{stop}}}{x} \right)^2. \quad (42)$$

Therefore, when we take  $x_{\text{stop}} \rightarrow \infty$  with  $x/x_{\text{stop}}$  fixed, we are forced to take  $\sigma_H \rightarrow 0$ . Simply put, when  $x_{\text{stop}} \rightarrow \infty$ , energy is transported along geodesics which originate asymptotically close to the string endpoint. Only these geodesics propagate to distances  $x = O(x_{\text{stop}})$ . This behavior can clearly be seen in Fig. 10.

Therefore, to get the energy loss rate we may expand Eq. (37) about  $\sigma_H \sim \sigma_* \rightarrow 0$ . The function  $\psi(\sigma)$  may be approximated by  $\psi(\sigma) \approx \psi'(\sigma_*)(\sigma - \sigma_*)$ . Hence, near the string endpoint

$$\Pi_0^\tau \approx -\frac{T_0}{\sigma^2 \sqrt{2\epsilon \psi'(\sigma_*)(\sigma - \sigma_*)}}. \quad (43)$$

The energy loss will depend on the unknown parameter  $\psi'(\sigma_*)$  which can be repackaged in terms of the initial energy

$$E(x=0) = \frac{\pi T_0}{2\sigma_*^{3/2} \sqrt{2\epsilon\psi'(\sigma_*)}} + O(1/\sqrt{\sigma_*}). \quad (44)$$

Substituting (43) and (41) into (37) and dividing by (44) we then secure<sup>109</sup>

$$\frac{1}{E(x=0)} \frac{dE}{dx} = - \frac{4x^2}{\pi x_{\text{stop}}^2 \sqrt{x_{\text{stop}}^2 - x^2}}. \quad (45)$$

Eq. (45) together with the stopping distance (26) provides a complete description of energy loss in terms of the initial energy, 't Hooft coupling  $\lambda$  and temperature  $T$ .

We now return to the boundary interpretation of  $dE/dx$ . It turns out that it is possible to solve the gravitational backreaction problem analytically in the long wavelength limit.<sup>d</sup> In doing so the hydrodynamic limit of the stress tensor  $T_{\text{hydro}}^{\mu\nu}$  can be extracted from the gravitational field perturbation in closed form. How is the string energy loss rate (45) encoded in  $T_{\text{hydro}}^{\mu\nu}$ ? The answer is

$$\partial_\mu T_{\text{hydro}}^{\mu\nu} = f^\nu(x) \delta^3(\mathbf{x} - \hat{x}t), \quad (46)$$

with  $f^0 = f^x = \frac{dE}{dx} \theta(x_{\text{stop}} - x)$ . Simply put, the energy loss rate (45) describes the rate in which energy is transferred from the jet to hydrodynamic modes.

The light quark energy loss rate (45) stands in stark contrast to the heavy quark counterpart (24). Heavy quarks lose most of their energy in the early stages of their trajectory when they are moving fastest. In contrast, from (45) we see that the light quark energy loss rate actually increases as  $x$  increases! This behavior, which was first pointed out in,<sup>93</sup> is reminiscent of a Bragg peak where the energy loss rate near thermalization is highest. Indeed, the energy loss rate (45) diverges as  $x \rightarrow x_{\text{stop}}$ .<sup>e</sup>

Recently the light quark energy loss rate (45) was employed in a phenomenological hybrid model of jet quenching which included both strong and weak coupling physics.<sup>78,79</sup> In the hybrid model the jet consists of a shower of partons which can split as the jet evolves. The splitting events were treated using perturbative QCD. Via soft interactions, in between splittings the partons can interact with the thermal medium and lose energy. The energy loss rate of the individual partons was treated using the light quark energy loss rate (45). The coefficient of the  $E^{1/3}$  scaling in the stopping distance (26) was allowed to vary providing a one parameter fit to data. This gave a good fit to the data provided that the resulting stopping distances are a factor 3 to 4 times larger in QCD than that in SYM at the same temperature and energy. This is natural since SYM has more degrees of freedom for energetic partons to interact with than QCD.

<sup>d</sup> This will be expanded upon in a coming paper.

<sup>e</sup> The rate that energy flows into hydrodynamic modes is only defined over time and length scales  $\gg 1/T$ . As such (45) should be regarded as the gradient expansion of the instantaneous jet energy loss rate. The gradient expansion of a function  $f(x)$  can diverge even if  $f(x)$  is itself finite. Hence, the instantaneous energy loss rate need not diverge as  $x \rightarrow x_{\text{stop}}$ .



## 6. Discussion with future perspectives

We hope to have shown some remarkable applications of holography to heavy ion collisions, while emphasizing that these results were obtained in a theory quite different from QCD itself. Most notably almost all results are obtained in the limit of infinitely strong coupling. Nevertheless, many of the works presented promise to have a degree of universality: they may apply to a large range of strongly coupled gauge theories. One particular example of such a hope is figure 6, which could display a universal rapidity profile of the plasma formed in high energy collisions in a strongly coupled gauge theories. Indications are that this profile can match experimental data for RHIC energies, while being perhaps too narrow at LHC energies.

The latter may also be expected; it was already known that LHC collisions did not agree well with the holographic prediction of the total multiplicity of charged particles,<sup>59,61</sup> as expanded upon in subsection 3.2. One natural explanation would be that at such high energies the coupling constant is intermediate, thereby invalidating the assumption of an infinitely strong coupling. Indeed models with weak coupling tend to give wider rapidity distributions, so from RHIC to LHC we may be watching a cross-over. On the other hand it is necessary to make the AdS/CFT models more realistic before drawing a firm conclusion, which can for instance be done by having less symmetry, preferably containing event-by-event fluctuations in the initial profile.

While this review naturally restricts to heavy ion collisions, we also wish to mention that holography is used for a much broader range of strongly coupled systems. These include non-fermi liquids<sup>110</sup> and holographic superconductors,<sup>111</sup> whereby the latter are believed to possibly have some relation with high temperature superconductors.

Lastly, we wish to express our excitement for the coming time, with several new experimental runs with different energies, different nuclei and higher statistics. Including features such as event-by-event distributions, non-trivial correlations, rare photon jets will give a very constraining data set, which will make it possible to distinguish all scenarios presented. This will hopefully give major lessons for both QCD, quark-gluon plasma physics, and applications of the gauge/gravity duality in a broad sense.

## Acknowledgments

We thank Krishna Rajagopal for interesting discussions and comments on the manuscript. WS wishes to thank Michal Heller, David Mateos, Jorge Casalderrey, Paul Romatschke and Scott Pratt for collaborations on much of the work presented here. PC is supported by the Fundamental Laws Initiative of the Center for the Fundamental Laws of Nature at Harvard University. WS is supported by the U.S. Department of Energy under grant Contract Number DE-SC0011090.

## References

1. J. M. Maldacena, The Large N limit of superconformal field theories and supergravity, *AIP Conf.Proc.* **484**, 51–63, (1999). doi: 10.1063/1.59653,10.1023/A:1026654312961.
2. K. Aamodt et al., Elliptic flow of charged particles in Pb-Pb collisions at 2.76 TeV, *Phys.Rev.Lett.* **105**, 252302, (2010). doi: 10.1103/PhysRevLett.105.252302.
3. E. Witten, Anti-de Sitter space, thermal phase transition, and confinement in gauge theories, *Adv.Theor.Math.Phys.* **2**, 505–532, (1998).
4. A. Karch and E. Katz, Adding flavor to AdS / CFT, *JHEP.* **0206**, 043, (2002). doi: 10.1088/1126-6708/2002/06/043.
5. E. Witten, Anti-de Sitter space and holography, *Adv.Theor.Math.Phys.* **2**, 253–291, (1998).
6. O. Aharony, S. S. Gubser, J. M. Maldacena, H. Ooguri, and Y. Oz, Large N field theories, string theory and gravity, *Phys.Rept.* **323**, 183–386, (2000). doi: 10.1016/S0370-1573(99)00083-6.
7. S. Hawking, Particle Creation by Black Holes, *Commun.Math.Phys.* **43**, 199–220, (1975). doi: 10.1007/BF02345020.
8. S. Bhattacharyya, V. E. Hubeny, S. Minwalla, and M. Rangamani, Nonlinear Fluid Dynamics from Gravity, *JHEP.* **0802**, 045, (2008). doi: 10.1088/1126-6708/2008/02/045.
9. V. E. Hubeny, S. Minwalla, and M. Rangamani, The fluid/gravity correspondence. (2011).
10. L. Landau and E. Lifshits, *Fluid Mechanics*, by L.D. Landau and E.M. Lifshitz. Teoreticheskai? fizika, (Pergamon Press, 1959). URL <http://books.google.com/books?id=CVbntgAACAAJ>.
11. C. Eckart, The Thermodynamics of irreversible processes. 3.. Relativistic theory of the simple fluid, *Phys.Rev.* **58**, 919–924, (1940). doi: 10.1103/PhysRev.58.919.
12. P. B. Arnold, G. D. Moore, and L. G. Yaffe, Transport coefficients in high temperature gauge theories. 1. Leading log results, *JHEP.* **0011**, 001, (2000). doi: 10.1088/1126-6708/2000/11/001.
13. H. B. Meyer, Transport Properties of the Quark-Gluon Plasma: A Lattice QCD Perspective, *Eur.Phys.J.* **A47**, 86, (2011). doi: 10.1140/epja/i2011-11086-3.
14. G. Policastro, D. Son, and A. Starinets, The Shear viscosity of strongly coupled N=4 supersymmetric Yang-Mills plasma, *Phys.Rev.Lett.* **87**, 081601, (2001). doi: 10.1103/PhysRevLett.87.081601.
15. P. Kovtun, D. T. Son, and A. O. Starinets, Viscosity in strongly interacting quantum field theories from black hole physics, *Phys.Rev.Lett.* **94**, 111601, (2005). doi: 10.1103/PhysRevLett.94.111601.
16. Y. Kats and P. Petrov, Effect of curvature squared corrections in AdS on the viscosity of the dual gauge theory, *JHEP.* **0901**, 044, (2009). doi: 10.1088/1126-6708/2009/01/044.
17. A. Buchel, J. T. Liu, and A. O. Starinets, Coupling constant dependence of the shear viscosity in N=4 supersymmetric Yang-Mills theory, *Nucl.Phys.* **B707**, 56–68, (2005). doi: 10.1016/j.nuclphysb.2004.11.055.
18. A. Buchel, Resolving disagreement for  $\eta/s$  in a CFT plasma at finite coupling, *Nucl.Phys.* **B803**, 166–170, (2008). doi: 10.1016/j.nuclphysb.2008.05.024.
19. R. C. Myers, M. F. Paulos, and A. Sinha, Quantum corrections to  $\eta/s$ , *Phys.Rev.* **D79**, 041901, (2009). doi: 10.1103/PhysRevD.79.041901.
20. P. Romatschke and U. Romatschke, Viscosity Information from Relativistic Nuclear Collisions: How Perfect is the Fluid Observed at RHIC?, *Phys.Rev.Lett.* **99**, 172301,

- (2007). doi: 10.1103/PhysRevLett.99.172301.
21. U. Heinz, C. Shen, and H. Song, The viscosity of quark-gluon plasma at RHIC and the LHC, *AIP Conf.Proc.* **1441**, 766–770, (2012). doi: 10.1063/1.3700674.
  22. B. Schenke, P. Tribedy, and R. Venugopalan, Event-by-event gluon multiplicity, energy density, and eccentricities in ultrarelativistic heavy-ion collisions, *Phys.Rev.* **C86**, 034908, (2012). doi: 10.1103/PhysRevC.86.034908.
  23. C. Gale, S. Jeon, B. Schenke, P. Tribedy, and R. Venugopalan, Event-by-event anisotropic flow in heavy-ion collisions from combined Yang-Mills and viscous fluid dynamics, *Phys.Rev.Lett.* **110**, 012302, (2013). doi: 10.1103/PhysRevLett.110.012302.
  24. M. Luzum and P. Romatschke, Conformal Relativistic Viscous Hydrodynamics: Applications to RHIC results at  $\sqrt{s(NN)} = 200$ -GeV, *Phys.Rev.* **C78**, 034915, (2008). doi: 10.1103/PhysRevC.78.034915, 10.1103/PhysRevC.79.039903.
  25. R. Baier, P. Romatschke, D. T. Son, A. O. Starinets, and M. A. Stephanov, Relativistic viscous hydrodynamics, conformal invariance, and holography, *JHEP.* **0804**, 100, (2008). doi: 10.1088/1126-6708/2008/04/100.
  26. R. Loganayagam, Entropy Current in Conformal Hydrodynamics, *JHEP.* **0805**, 087, (2008). doi: 10.1088/1126-6708/2008/05/087.
  27. J. Erdmenger, M. Haack, M. Kaminski, and A. Yarom, Fluid dynamics of R-charged black holes, *JHEP.* **0901**, 055, (2009). doi: 10.1088/1126-6708/2009/01/055.
  28. R. P. Geroch, Relativistic theories of dissipative fluids, *J.Math.Phys.* **36**, 4226, (1995). doi: 10.1063/1.530958.
  29. W. A. Hiscock and L. Lindblom, Generic instabilities in first-order dissipative relativistic fluid theories, *Phys.Rev.* **D31**, 725–733, (1985). doi: 10.1103/PhysRevD.31.725.
  30. I. Muller, Zum Paradoxon der Wärmeleitungstheorie, *Z.Phys.* **198**, 329–344, (1967). doi: 10.1007/BF01326412.
  31. W. Israel and J. Stewart, Transient relativistic thermodynamics and kinetic theory, *Annals Phys.* **118**, 341–372, (1979). doi: 10.1016/0003-4916(79)90130-1.
  32. R. Baier and P. Romatschke, Causal viscous hydrodynamics for central heavy-ion collisions, *Eur.Phys.J.* **C51**, 677–687, (2007). doi: 10.1140/epjc/s10052-007-0308-5.
  33. P. Romatschke, New Developments in Relativistic Viscous Hydrodynamics, *Int.J.Mod.Phys.* **E19**, 1–53, (2010). doi: 10.1142/S0218301310014613.
  34. H. Song and U. W. Heinz, Suppression of elliptic flow in a minimally viscous quark-gluon plasma, *Phys.Lett.* **B658**, 279–283, (2008). doi: 10.1016/j.physletb.2007.11.019.
  35. M. P. Heller, R. A. Janik, and P. Witaszczyk, On the character of hydrodynamic gradient expansion in gauge theory plasma, *Phys.Rev.Lett.* **110**, 211602, (2013). doi: 10.1103/PhysRevLett.110.211602.
  36. N. Banerjee, J. Bhattacharya, S. Bhattacharyya, S. Dutta, R. Loganayagam, et al., Hydrodynamics from charged black branes, *JHEP.* **1101**, 094, (2011). doi: 10.1007/JHEP01(2011)094.
  37. D. Kharzeev and A. Zhitnitsky, Charge separation induced by P-odd bubbles in QCD matter, *Nucl.Phys.* **A797**, 67–79, (2007). doi: 10.1016/j.nuclphysa.2007.10.001.
  38. D. E. Kharzeev, The Chiral Magnetic Effect and Anomaly-Induced Transport, *Prog.Part.Nucl.Phys.* **75**, 133–151, (2014). doi: 10.1016/j.ppnp.2014.01.002.
  39. Y. Hirono, T. Hirano, and D. E. Kharzeev, The chiral magnetic effect in heavy-ion collisions from event-by-event anomalous hydrodynamics. (2014).
  40. D. T. Son and P. Surowka, Hydrodynamics with Triangle Anomalies, *Phys.Rev.Lett.* **103**, 191601, (2009). doi: 10.1103/PhysRevLett.103.191601.

41. A. Gynther, K. Landsteiner, F. Pena-Benitez, and A. Rebhan, Holographic Anomalous Conductivities and the Chiral Magnetic Effect, *JHEP.* **1102**, 110, (2011). doi: 10.1007/JHEP02(2011)110.
42. S. S. Gubser, Symmetry constraints on generalizations of Bjorken flow, *Phys.Rev.* **D82**, 085027, (2010). doi: 10.1103/PhysRevD.82.085027.
43. G. S. Denicol, U. W. Heinz, M. Martinez, J. Noronha, and M. Strickland, New Exact Solution of the Relativistic Boltzmann Equation and its Hydrodynamic Limit, *Phys.Rev.Lett.* **113**(20), 202301, (2014). doi: 10.1103/PhysRevLett.113.202301.
44. L. Lehner, Numerical relativity: A Review, *Class.Quant.Grav.* **18**, R25–R86, (2001). doi: 10.1088/0264-9381/18/17/202.
45. F. Pretorius, Evolution of binary black hole spacetimes, *Phys.Rev.Lett.* **95**, 121101, (2005). doi: 10.1103/PhysRevLett.95.121101.
46. P. M. Chesler and L. G. Yaffe, Numerical solution of gravitational dynamics in asymptotically anti-de Sitter spacetimes. (2013).
47. G. T. Horowitz and V. E. Hubeny, Quasinormal modes of AdS black holes and the approach to thermal equilibrium, *Phys.Rev.* **D62**, 024027, (2000). doi: 10.1103/PhysRevD.62.024027.
48. P. M. Chesler and L. G. Yaffe, Horizon formation and far-from-equilibrium isotropization in supersymmetric Yang-Mills plasma, *Phys.Rev.Lett.* **102**, 211601, (2009). doi: 10.1103/PhysRevLett.102.211601.
49. P. M. Chesler and L. G. Yaffe, Boost invariant flow, black hole formation, and far-from-equilibrium dynamics in  $N = 4$  supersymmetric Yang-Mills theory, *Phys.Rev.* **D82**, 026006, (2010). doi: 10.1103/PhysRevD.82.026006.
50. M. P. Heller, R. A. Janik, and P. Witaszczyk, The characteristics of thermalization of boost-invariant plasma from holography, *Phys.Rev.Lett.* **108**, 201602, (2012). doi: 10.1103/PhysRevLett.108.201602.
51. M. P. Heller, D. Mateos, W. van der Schee, and D. Trancanelli, Strong Coupling Isotropization of Non-Abelian Plasmas Simplified, *Phys.Rev.Lett.* **108**, 191601, (2012). doi: 10.1103/PhysRevLett.108.191601.
52. M. P. Heller, D. Mateos, W. van der Schee, and M. Triana, Holographic isotropization linearized, *JHEP.* **1309**, 026, (2013). doi: 10.1007/JHEP09(2013)026.
53. D. Steineder, S. A. Stricker, and A. Vuorinen, Holographic Thermalization at Intermediate Coupling, *Phys.Rev.Lett.* **110**(10), 101601, (2013). doi: 10.1103/PhysRevLett.110.101601.
54. S. A. Stricker, Holographic thermalization in  $N=4$  Super Yang-Mills theory at finite coupling. (2013). doi: 10.1140/epjc/s10052-014-2727-4.
55. J. Bjorken, Highly Relativistic Nucleus-Nucleus Collisions: The Central Rapidity Region, *Phys.Rev.* **D27**, 140–151, (1983). doi: 10.1103/PhysRevD.27.140.
56. W. van der Schee, *Gravitational collisions and the quark-gluon plasma*. PhD thesis, Utrecht University, (2014).
57. R. A. Janik and R. B. Peshanski, Asymptotic perfect fluid dynamics as a consequence of AdS/CFT, *Phys.Rev.* **D73**, 045013, (2006). doi: 10.1103/PhysRevD.73.045013.
58. J. L. Albacete, Y. V. Kovchegov, and A. Taliotis, Modeling Heavy Ion Collisions in AdS/CFT, *JHEP.* **0807**, 100, (2008). doi: 10.1088/1126-6708/2008/07/100.
59. S. S. Gubser, S. S. Pufu, and A. Yarom, Entropy production in collisions of gravitational shock waves and of heavy ions, *Phys.Rev.* **D78**, 066014, (2008). doi: 10.1103/PhysRevD.78.066014.
60. D. Grumiller and P. Romatschke, On the collision of two shock waves in AdS(5), *JHEP.* **0808**, 027, (2008). doi: 10.1088/1126-6708/2008/08/027.

61. S. Lin and E. Shuryak, Grazing Collisions of Gravitational Shock Waves and Entropy Production in Heavy Ion Collision, *Phys.Rev.* **D79**, 124015, (2009). doi: 10.1103/PhysRevD.79.124015.
62. I. Y. Aref'eva, A. Bagrov, and E. Guseva, Critical Formation of Trapped Surfaces in the Collision of Non-expanding Gravitational Shock Waves in de Sitter Space-Time, *JHEP.* **0912**, 009, (2009). doi: 10.1088/1126-6708/2009/12/009.
63. T. Dray and G. 't Hooft, The Gravitational Shock Wave of a Massless Particle, *Nucl.Phys.* **B253**, 173, (1985). doi: 10.1016/0550-3213(85)90525-5.
64. B. Muller and K. Rajagopal, From entropy and jet quenching to deconfinement?, *Eur.Phys.J.* **C43**, 15–21, (2005). doi: 10.1140/epjc/s2005-02256-3.
65. A. Toia, Bulk Properties of Pb-Pb collisions at  $\sqrt{s_{NN}} = 2.76$  TeV measured by ALICE, *J.Phys.* **G38**, 124007, (2011). doi: 10.1088/0954-3899/38/12/124007.
66. P. M. Chesler and L. G. Yaffe, Holography and colliding gravitational shock waves in asymptotically AdS<sub>5</sub> spacetime, *Phys.Rev.Lett.* **106**, 021601, (2011). doi: 10.1103/PhysRevLett.106.021601.
67. J. Casalderrey-Solana, M. P. Heller, D. Mateos, and W. van der Schee, From full stopping to transparency in a holographic model of heavy ion collisions, *Phys. Rev. Lett.* **111**, **181601**, (2013). doi: 10.1103/PhysRevLett.111.181601.
68. P. Arnold, P. Romatschke, and W. van der Schee, Absence of a local rest frame in far from equilibrium quantum matter, *JHEP.* **1410**, 110, (2014). doi: 10.1007/JHEP10(2014)110.
69. S. S. Gubser and W. van der Schee, Complexified boost invariance and holographic heavy ion collisions, *JHEP.* **01**, 028, (2014). doi: 10.1007/JHEP10(2014)110.
70. J. Casalderrey-Solana, M. P. Heller, D. Mateos, and W. van der Schee, Longitudinal Coherence in a Holographic Model of p-Pb Collisions. (2013).
71. M. P. Heller, R. A. Janik, and P. Witaszczyk, A numerical relativity approach to the initial value problem in asymptotically Anti-de Sitter spacetime for plasma thermalization - an ADM formulation, *Phys.Rev.* **D85**, 126002, (2012). doi: 10.1103/PhysRevD.85.126002.
72. W. van der Schee, Holographic thermalization with radial flow, *Phys.Rev.* **D87**, 061901, (2013). doi: 10.1103/PhysRevD.87.061901.
73. W. van der Schee, P. Romatschke, and S. Pratt, A fully dynamical simulation of central nuclear collisions, *Phys.Rev.Lett.* **111**, 222302, (2013). doi: 10.1103/PhysRevLett.111.222302.
74. M. Habich, J. Nagle, and P. Romatschke, Particle spectra and HBT radii for simulated central nuclear collisions of C+C, Al+Al, Cu+Cu, Au+Au, and Pb+Pb from  $\sqrt{s}=62.4-2760$  GeV. (2014).
75. J. Vredevoogd and S. Pratt, Universal Flow in the First Stage of Relativistic Heavy Ion Collisions, *Phys.Rev.* **C79**, 044915, (2009). doi: 10.1103/PhysRevC.79.044915.
76. B. Abelev et al., Pion, Kaon, and Proton Production in Central Pb–Pb Collisions at  $\sqrt{s_{NN}} = 2.76$  TeV, *Phys.Rev.Lett.* **109**, 252301, (2012). doi: 10.1103/PhysRevLett.109.252301.
77. J. Casalderrey-Solana, E. Shuryak, and D. Teaney, Hydrodynamic flow from fast particles. (2006).
78. J. Casalderrey-Solana, D. C. Gulhan, J. G. Milhano, D. Pablos, and K. Rajagopal, A Hybrid Strong/Weak Coupling Approach to Jet Quenching, *JHEP.* **1410**, 19, (2014). doi: 10.1007/JHEP10(2014)019.
79. J. Casalderrey-Solana, D. C. Gulhan, J. G. Milhano, D. Pablos, and K. Rajagopal, Jet quenching within a hybrid strong/weak coupling approach, *Nucl.Phys.* **A931**, 487–492, (2014). doi: 10.1016/j.nuclphysa.2014.09.019.

80. A. Adare et al., Energy Loss and Flow of Heavy Quarks in Au+Au Collisions at  $\sqrt{s_{NN}} = 200$ -GeV, *Phys.Rev.Lett.* **98**, 172301, (2007). doi: 10.1103/PhysRevLett.98.172301.
81. S. Adler et al., Dense-Medium Modifications to Jet-Induced Hadron Pair Distributions in Au+Au Collisions at  $\sqrt{s_{NN}} = 200$ -GeV, *Phys.Rev.Lett.* **97**, 052301, (2006). doi: 10.1103/PhysRevLett.97.052301.
82. S. Chatrchyan et al., Observation and studies of jet quenching in PbPb collisions at nucleon-nucleon center-of-mass energy = 2.76 TeV, *Phys.Rev.* **C84**, 024906, (2011). doi: 10.1103/PhysRevC.84.024906.
83. G. Aad et al., Observation of a Centrality-Dependent Dijet Asymmetry in Lead-Lead Collisions at  $\sqrt{s_{NN}} = 2.77$  TeV with the ATLAS Detector at the LHC, *Phys.Rev.Lett.* **105**, 252303, (2010). doi: 10.1103/PhysRevLett.105.252303.
84. W. T. Giele, D. A. Kosower, and P. Z. Skands, A simple shower and matching algorithm, *Phys.Rev.* **D78**, 014026, (2008). doi: 10.1103/PhysRevD.78.014026.
85. D. M. Hofman and J. Maldacena, Conformal collider physics: Energy and charge correlations, *JHEP.* **0805**, 012, (2008). doi: 10.1088/1126-6708/2008/05/012.
86. C. Athanasiou, P. M. Chesler, H. Liu, D. Nickel, and K. Rajagopal, Synchrotron radiation in strongly coupled conformal field theories, *Phys.Rev.* **D81**, 126001, (2010). doi: 10.1103/PhysRevD.81.126001, 10.1103/PhysRevD.84.069901.
87. Y. Hatta, E. Iancu, A. Mueller, and D. Triantafyllopoulos, Radiation by a heavy quark in  $N=4$  SYM at strong coupling, *Nucl.Phys.* **B850**, 31–52, (2011). doi: 10.1016/j.nuclphysb.2011.04.011.
88. P. M. Chesler, Y.-Y. Ho, and K. Rajagopal, Shining a Gluon Beam Through Quark-Gluon Plasma, *Phys.Rev.* **D85**, 126006, (2012). doi: 10.1103/PhysRevD.85.126006.
89. P. Arnold and D. Vaman, Jet quenching in hot strongly coupled gauge theories revisited: 3-point correlators with gauge-gravity duality, *JHEP.* **1010**, 099, (2010). doi: 10.1007/JHEP10(2010)099.
90. P. Arnold and D. Vaman, Jet quenching in hot strongly coupled gauge theories simplified, *JHEP.* **1104**, 027, (2011). doi: 10.1007/JHEP04(2011)027.
91. P. Arnold and D. Vaman, Some new results for 'jet' stopping in AdS/CFT: long version, *J.Phys.* **G38**, 124175, (2011). doi: 10.1088/0954-3899/38/12/124175.
92. P. M. Chesler, K. Jensen, and A. Karch, Jets in strongly-coupled  $N = 4$  super Yang-Mills theory, *Phys.Rev.* **D79**, 025021, (2009). doi: 10.1103/PhysRevD.79.025021.
93. P. M. Chesler, K. Jensen, A. Karch, and L. G. Yaffe, Light quark energy loss in strongly-coupled  $N = 4$  supersymmetric Yang-Mills plasma, *Phys.Rev.* **D79**, 125015, (2009). doi: 10.1103/PhysRevD.79.125015.
94. C. Herzog, A. Karch, P. Kovtun, C. Kozcaz, and L. Yaffe, Energy loss of a heavy quark moving through  $N=4$  supersymmetric Yang-Mills plasma, *JHEP.* **0607**, 013, (2006). doi: 10.1088/1126-6708/2006/07/013.
95. S. S. Gubser, Drag force in AdS/CFT, *Phys.Rev.* **D74**, 126005, (2006). doi: 10.1103/PhysRevD.74.126005.
96. J. Casalderrey-Solana and D. Teaney, Heavy quark diffusion in strongly coupled  $N=4$  Yang-Mills, *Phys.Rev.* **D74**, 085012, (2006). doi: 10.1103/PhysRevD.74.085012.
97. P. M. Chesler and L. G. Yaffe, The Wake of a quark moving through a strongly-coupled plasma, *Phys.Rev.Lett.* **99**, 152001, (2007). doi: 10.1103/PhysRevLett.99.152001.
98. P. M. Chesler and L. G. Yaffe, The Stress-energy tensor of a quark moving through a strongly-coupled  $N=4$  supersymmetric Yang-Mills plasma: Comparing hydrodynamics and AdS/CFT, *Phys.Rev.* **D78**, 045013, (2008). doi: 10.1103/PhysRevD.78.045013.

99. S. S. Gubser, S. S. Pufu, and A. Yarom, Sonic booms and diffusion wakes generated by a heavy quark in thermal AdS/CFT, *Phys.Rev.Lett.* **100**, 012301, (2008). doi: 10.1103/PhysRevLett.100.012301.
100. J. J. Friess, S. S. Gubser, G. Michalogiorgakis, and S. S. Pufu, The Stress tensor of a quark moving through N=4 thermal plasma, *Phys.Rev.* **D75**, 106003, (2007). doi: 10.1103/PhysRevD.75.106003.
101. A. Ficnar, J. Noronha, and M. Gyulassy, Jet Quenching in Non-Conformal Holography, *J.Phys.* **G38**, 124176, (2011). doi: 10.1088/0954-3899/38/12/124176.
102. M. Chernicoff, D. Fernandez, D. Mateos, and D. Trancanelli, Jet quenching in a strongly coupled anisotropic plasma, *JHEP.* **1208**, 041, (2012). doi: 10.1007/JHEP08(2012)041.
103. P. M. Chesler, M. Lekaveckas, and K. Rajagopal, Heavy quark energy loss far from equilibrium in a strongly coupled collision, *JHEP.* **1310**, 013, (2013). doi: 10.1007/JHEP10(2013)013.
104. M. Chernicoff and A. Guijosa, Acceleration, Energy Loss and Screening in Strongly-Coupled Gauge Theories, *JHEP.* **0806**, 005, (2008). doi: 10.1088/1126-6708/2008/06/005.
105. J. Casalderrey-Solana and D. Teaney, Transverse Momentum Broadening of a Fast Quark in a N=4 Yang Mills Plasma, *JHEP.* **0704**, 039, (2007). doi: 10.1088/1126-6708/2007/04/039.
106. S. S. Gubser, Momentum fluctuations of heavy quarks in the gauge-string duality, *Nucl.Phys.* **B790**, 175–199, (2008). doi: 10.1016/j.nuclphysb.2007.09.017.
107. S. S. Gubser, D. R. Gulotta, S. S. Pufu, and F. D. Rocha, Gluon energy loss in the gauge-string duality, *JHEP.* **0810**, 052, (2008). doi: 10.1088/1126-6708/2008/10/052.
108. A. Ficnar and S. S. Gubser, Finite momentum at string endpoints, *Phys.Rev.* **D89**, 026002, (2014). doi: 10.1103/PhysRevD.89.026002.
109. P. M. Chesler and K. Rajagopal, Jet quenching in strongly coupled plasma. (2014).
110. T. Faulkner, H. Liu, J. McGreevy, and D. Vegh, Emergent quantum criticality, Fermi surfaces, and AdS(2), *Phys.Rev.* **D83**, 125002, (2011). doi: 10.1103/PhysRevD.83.125002.
111. S. A. Hartnoll, C. P. Herzog, and G. T. Horowitz, Building a Holographic Superconductor, *Phys.Rev.Lett.* **101**, 031601, (2008). doi: 10.1103/PhysRevLett.101.031601.